

Published in final edited form as:

*Nat Biotechnol.* 2011 April ; 29(4): 352–356. doi:10.1038/nbt.1764.

## Fluorescent peptides highlight peripheral nerves during surgery in mice

Michael A Whitney<sup>1</sup>, Jessica L Crisp<sup>2</sup>, Linda T Nguyen<sup>3</sup>, Beth Friedman<sup>1</sup>, Larry A Gross<sup>4</sup>, Paul Steinbach<sup>4</sup>, Roger Y Tsien<sup>1,2,4</sup>, and Quyen T Nguyen<sup>3</sup>

<sup>1</sup>Department of Pharmacology, University of California at San Diego, La Jolla, California, USA.

<sup>2</sup>Department of Chemistry and Biochemistry, University of California at San Diego, La Jolla, California, USA.

<sup>3</sup>Division of Otolaryngology-Head and Neck Surgery, University of California at San Diego, La Jolla, California, USA.

<sup>4</sup>Howard Hughes Medical Institute, University of California at San Diego, La Jolla, California, USA.

### Abstract

Nerve preservation is an important goal during surgery because accidental transection or injury leads to significant morbidity, including numbness, pain, weakness or paralysis. Nerves are usually identified by their appearance and relationship to nearby structures or detected by local electrical stimulation (electromyography), but thin or buried nerves are sometimes overlooked. Here, we use phage display to select a peptide that binds preferentially to nerves. After systemic injection of a fluorescently labeled version of the peptide in mice, all peripheral nerves are clearly delineated within 2 h. Contrast between nerve and adjacent tissue is up to tenfold, and useful contrast lasts up to 8 h. No changes in behavior or activity are observed after treatment, indicating a lack of obvious toxicity. The fluorescent probe also labels nerves in human tissue samples. Fluorescence highlighting is independent of axonal integrity, suggesting that the probe could facilitate surgical repair of injured nerves and help prevent accidental transection.

Accidental transection or injury of nerves during surgery can lead to significant patient morbidity including chronic pain or permanent paralysis. Thin or buried nerves are particularly difficult to distinguish and are therefore the most likely to be damaged during surgical procedures.

Identification of motor nerves before direct exposure is currently dependent on electromyographic (EMG) monitoring<sup>1–3</sup>, in which a stimulating electrode is inserted and

© 2011 Nature America, Inc. All rights reserved.

Correspondence should be addressed to Q.T.N. (quyennguyen@ucsd.edu).

Note: Supplementary information is available on the Nature Biotechnology website.

#### AUTHOR CONTRIBUTIONS

M.A.W. designed and performed experiments, interpreted data and wrote manuscript. J.L.C. designed and performed experiments and interpreted data. L.T.N. designed and performed experiments and interpreted data. B.F. designed and performed experiments and interpreted data. L.A.G. designed and performed experiments and interpreted data. P.S. provided computer support for experiments, R.Y.T. designed experiments, interpreted data and wrote manuscript. Q.T.N. designed and performed experiments, interpreted data and wrote manuscript.

#### COMPETING FINANCIAL INTERESTS

The authors declare competing financial interests: details accompany the full-text HTML version of the paper at <http://www.nature.com/naturebiotechnology/>.

distal muscle twitches are monitored. EMG is not an imaging technique, so even if a nerve has been identified in one location, there is no visual guidance for how far from the stimulation site the nerve lies. Furthermore, EMG identifies only motor pathways, not sensory fibers such as the first two divisions of the trigeminal nerves, the cochleovestibular nerve or the neurovascular bundle surrounding the prostate gland<sup>4,5</sup>, where nerve injury during radical prostatectomy leads to significant urinary incontinence and erectile dysfunction<sup>6</sup>. Finally, EMG fails if axonal or neuromuscular transmission is temporarily blocked distal to the recording site by nerve compression, trauma, tumor invasion, local anesthetics or neuromuscular blockers. Although there are developing technologies for *in vivo* nerve visualization such as optical coherence tomography<sup>7</sup> or laser confocal microscopy<sup>8</sup>, these techniques have focused on the visualization of the optic or other superficial nerves and may not be generally applicable for viewing nerves in a surgical setting.

Current methods for nerve labeling during surgery depend on retrograde or anterograde tracing of individual axonal tracts using fluorescent dyes<sup>9–12</sup>. The dyes are applied either to the innervations target and travel in a retrograde fashion to label the innervating nerve fibers or directly to identified nerves and label nerve fibers in both anterograde and retrograde directions. Local injections have the drawback of only labeling one nerve fiber tract at a time and that axonal labeling is limited. Axonal transport is relatively slow and it can take days to label a single human nerve. Furthermore, the direct injection of fluorescent dyes contaminates the surgical site with excess fluorescent dyes and may be damaging to the target organs or nerve of interest.

In this study, we describe the development of peptides by phage display<sup>13</sup> that preferentially bind to peripheral nerve tissue compared to adjacent non-nerve tissue after systemic administration.

We used *in vitro* selection with either excised murine peripheral nerves or purified myelin basic protein (MBP) and *in vivo* selection where phage were injected into living mice and nerves were harvested for phage isolation. From the *in vitro* selection against MBP, a single phage with its variable sequence coding for the peptide TYTDWLNFWAWP (NP39) was identified (Supplementary Fig. 1).

The *in vitro* selection against excised peripheral nerves yielded three sequences that were repeatedly observed. Of 14 specific phage sequences at the end of seven rounds of selection, 5 coded for NTQTLAKAPEHT (NP41), 3 for KSLSRHDHIIHHH (NP40) and 2 for DFTKTSPLGIH (NP42). The remaining phage sequences were each represented only once (Supplementary Fig. 1). The *in vivo* selection did not yield any duplicated phage after eight rounds of selection, perhaps because vigorous washing to remove mechanically entangled or loosely bound phage is not possible in a live animal. One sequence selected *in vivo*, AHHNSWKAKHHS (NP38), was chosen for further testing because it contained multiple histidines reminiscent of NP40. Both NP40 and NP38 have been previously identified in various phage selection schemes for binding to proteins (scFV, GST-FLAS-DRD) or hepatoma cell lines, which could indicate that these peptides either bind nonspecifically to proteins or cells or alternatively that they bind to substrates common to both screens<sup>14–17</sup>.

Sequences NP38, 40, 41, 42 and a control peptide containing the shared amino acids in random order were similarly synthesized as fluorescein-5(6)-carbonyl group (FAM) conjugates on a C-terminal lysinamide. To test nerve binding affinity *in vivo* of each of the identified sequences, we injected FAM-labeled peptides intravenously into living mice and evaluated the contrast between nerve and muscle 2–4 h after injection. The sequence identified through *in vitro* selection against MBP (NP39) and the sequence identified

through the *in vivo* selection (NP38) did not have significant nerve-to-muscle contrast and both showed high-background binding to the surrounding nonneural tissue. The peptide sequence identified most often in *in vitro* selection against excised nerves NP41 had the best nerve to nonnerve contrast. The other two sequences, NP40 and NP42, identified through this same selection strategy also yielded some nerve-to-muscle contrast, although less than that of NP41 (Supplementary Table 1). A systemic survey of animals injected with FAM-NP41 revealed that all peripheral nerves and their arborizations (including nerve branches as small as 50  $\mu$ m in diameter) were brightly labeled, including motor pathways, and sensory nerves such as the first two divisions of the trigeminal nerves (Fig. 1). The central nervous system did not appear to take up any fluorescence, perhaps because the peptide did not cross the blood-brain barrier.

To evaluate the kinetics of peptide nerve binding *in vivo*, we imaged sciatic nerves and surrounding nonnerve tissue in mice before and after intravenous administration of FAM-NP41. Before administration of the peptide, there was little contrast between the nerve (small yellow arrowheads) and surrounding nonnerve tissue (Supplementary Fig. 2a). Within seconds after intravenous administration of FAM-NP41, fluorescence could be seen leaking from capillaries (arrows) associated with the sciatic nerves (insert, Supplementary Fig. 2b). Nerve fluorescence peaked at 10 min after administration (Supplementary Fig. 2c) and declined thereafter to a plateau (Fig. 2a). Muscle fluorescence was highest immediately after intravenous administration of the peptide, with a half-life of  $\sim$ 20 min ( $n = 5$ , Fig. 2a). Serum half-life was calculated at  $\sim$ 10 min ( $n = 5$ , Fig. 2b). Useful contrast between nerve and surrounding tissue developed by 2 h after injection ( $n = 5$ , Fig. 2c and Supplementary Fig. 2e) and lasted several hours (Fig. 2a,c and Supplementary Fig. 2e,f), reaching seven- to tenfold by 4–5 h ( $n = 5$ , Fig. 2c). By 24 h after injection, all visible staining had disappeared ( $n = 20$ ). Intravenous injection of the mirror-image peptide with all D-amino acids showed nerve staining at the level of carboxyfluorescein alone (Supplementary Fig. 3). The nerve-to-surrounding tissue contrast ratio was correlated with the amount of peptide administered over the range of 15 to 5,000 nmoles per mouse (Fig. 2d).

We attempted topical application of FAM-NP41 to label mouse sciatic nerves *in vivo*, however, incomplete wash-out of probe and residual fluorescence due to the probe infiltrating into tissue pockets led to the appearance of linear structures that could be mistaken for nerve fibers.

To evaluate the localization of NP41 binding within nerves, we injected peptide into thy1-YFP transgenic mice whose axons were genetically encoded with YFP under a neuron-specific promoter<sup>18</sup>. To avoid spectral overlap with YFP and to allow imaging deeper in tissues, we replaced FAM with the deep red fluorophore Cy5. Cy5-NP41 precisely labeled nerves that expressed YFP and correlated with nerve fibers as seen in brightfield imaging (Fig. 3a–c). No nerve-to-muscle contrast was detected in mice injected with unconjugated Cy5 (Supplementary Fig. 4a).

To confirm that changing the fluorophore does not change nerve distribution of NP41, we imaged frozen cross-sections of nerves from mice that had been injected with either 150 nmols FAM-NP41 or Cy5-NP41. Imaged cross-sections showed that labeling was comparable using the two fluorophores (Supplementary Fig. 4b,c). To determine if the NP41 was labeling axons, we imaged 3–5  $\mu$ m cryosections of nerves from thy1-YFP animals treated with Cy5-NP41. Cy5-NP41 localized to the epineurium of the nerves with some labeling of the perineurium and endoneurium, but did not colocalize with either myelin or axons (Fig. 3d–i).

To evaluate the ability of NP41 to highlight nerve branches that were buried within tissue, we compared visibility of standard white light reflectance and fluorescent images of Cy5-NP41 and YFP-labeled axons. Cy5-NP41 (Fig. 3c, insert arrows) was better than brightfield (Fig. 3a, insert) or YFP (Fig. 3b, insert) at highlighting nerves that were branching deep into muscle. Nerve branches not on the surface were essentially invisible with reflectance imaging (long arrow, arrowheads, Fig. 4a). However, these buried branches can be visualized with Cy5-NP41 (arrowheads and long arrow, Fig. 4b) and YFP (arrowheads, Fig. 4c).

We also assessed the visibility of nerve branches covered by breast cancer tumor in syngeneic graft models<sup>19,20</sup>. For this evaluation we co-administered Cy5-labeled dendrimer conjugates of activatable, cell-penetrating peptides (ACPPs), which highlight tumor margins and FAM-NP41 (refs. 19,20). As shown, nerve branches that descend into the tumor become invisible with reflectance imaging (arrowhead, Fig. 4d); however, these buried branches could be visualized, with FAM-NP41 (arrowhead, Fig. 4e) protruding into the tumor which has been labeled with Cy5 dendrimer (Fig. 4f). The ACPP marks the tumor to be excised, whereas the NP41 highlights the nerve tissue whose preservation is most essential.

Mice showed no change in behavior or activity after injections of 15–5,000 nmoles of FAM-NP41 or 75–300 nmoles Cy5-NP41. In addition, mice that had been injected with 15 nmoles ( $n = 2$ ), 45 nmoles ( $n = 2$ ), 150 nmoles ( $n = 2$ ), 450 nmoles ( $n = 2$ ), 5,000 nmoles ( $n = 1$ ) showed no significant weight changes or morbidity through 8 weeks of monitoring compared to uninjected mice ( $n = 2$ ). In addition, injection of 150 nmoles of FAM-NP41 had no effect on the shape, amplitude or latency of compound muscle action potential<sup>21</sup> (Supplementary Fig. 5), indicating NP41 has no acute effect on peripheral nerve conduction or neuromuscular transmission.

To evaluate the biodistribution of the peptide after systemic administration, organs were harvested from mice intravenously injected with 150 nmoles FAM-NP41 or Cy5-NP41 and fluorescence uptake was evaluated. The majority of the fluorescence accumulated in the kidney and was excreted into the urine. Liquid chromatography–electrospray mass spectrometry of the urine gave different peaks from normal mouse urine spiked with intact FAM-NP41 or Cy5-NP41, indicating that the injected peptides had been efficiently metabolized. The major fluorescently labeled species identified by matrix-assisted laser desorption/ionization mass spectrometry were cysteinamide-Cy5 and lysinamide-FAM from mice injected with Cy5-NP41 or FAM-NP41, respectively. Small fractions of successive fragments of NP41 starting from the C terminus were also recovered, suggesting that the entire peptide had been sequentially degraded from the N terminus (Supplementary Fig. 6c,d). In contrast, in urine from mice injected with control all  $\alpha$ -amino acid FAM-NP41, the full-length peptide was recovered intact (Supplementary Fig. 6e).

In addition to labeling healthy nerves during nontrauma related surgery, the ability to label and identify severed or injured nerves is also of considerable clinical utility. Such, visualization of injured or severed nerves could guide procedures such as rejoining severed nerves leading to better prognosis after injury. In the cases of injury involving motor nerves, EMG may fail because severed nerves typically lack functionality. Direct labeling could also prove useful when EMG detection does not work because swelling or inflammation leads to short-term loss of nerve conduction. Nerve labeling by FAM-NP41 was 100% of contralateral intact nerve immediately and 1 d after crush injury, decreased by 40% at day 3 and was back to 100% 7 d after injury (Supplementary Fig. 7a–f,i). Because we detected a transient decrease in uptake upon crush injury, we tested if this effect could potentially be due to a temporary decrease in blood flow to the nerve tissue thereby inhibiting uptake. As predicted, nerve devascularization (by intentional injury to the feeding vessels before

peptide administration) greatly diminished subsequent uptake of FAM-NP41 (Supplementary Fig. 7g,h).

To evaluate whether NP41 could highlight human as well as mouse nerves, freshly resected recurrent laryngeal nerves and adjacent muscle obtained from patients undergoing total laryngectomy were incubated with FAM-NP41. Selective binding of FAM-NP41 to nerves as compared to adjacent muscle was observed (Supplementary Fig. 8a,b). Histological examination of tissue sections showed that the fluorescence was concentrated in the connective tissue surrounding the nerve, that is, epineurium, perineurium and endoneurium (Supplementary Fig. 8c–h), similar to the binding pattern in murine nerves. Although we cannot administer NP41 to human subjects without much further testing and regulatory approval, these *ex vivo* tests provide preliminary evidence that NP41 could cross-react with human nerves.

The method of systemic injection of fluorescently labeled peptides to label nerves overcomes some of the major disadvantages of currently available fluorescent tracers, which provide only localized labeling, have low signal-to-noise ratio and require preoperative lead time incompatible with most surgical procedures.

Our peptide localizes predominantly to nerve-associated connective tissue and not to myelin or axonal membranes, which may explain why there were no pharmacological or toxic effects observed in our preliminary toxicity assessments. We achieve good contrast of all nerves in the body including motor and sensory nerves within 2–3 h compared to tracers that have to be transported in an anterograde or retrograde direction and can require days to label. Contrast from our systemically injected peptides lasts several hours, which would be long enough for most typical operations. A probe of this sort could potentially be further optimized to minimize wash-out time allowing the agents to be provided intravenously within minutes before skin incision. We believe that eventually the use of fluorescently labeled probes for nerve visualization will be routine and will decrease the incidence of inadvertent injury during surgery and may improve identification and repair of nerves after trauma thereby leading to improved patient prognosis.

We were able to detect nerve arborizations as small as 50  $\mu\text{m}$ , which is at least one order of magnitude smaller than most surgically relevant nerves in the human body. In addition, the peptide is cleared within 24 h and completely metabolized, which should reduce the chance of side effects. We would like to optimize NP41 and are therefore using a variety of methods to identify the molecular target(s) to which peptide NP41 binds. The identification of a specific target may allow setting up specific binding assays or using crystallographic information to determine structure-activity relationships and optimize NP41.

Even in the absence of a defined target, we can optimize for nerve affinity, decrease binding to negative tissues, shift fluorescence to longer wavelengths and modify pharmacology to improve contrast of NP41 or related molecules for improved *in vivo* imaging of nerves.

The minimal murine doses of NP41 used *in vivo* are currently equivalent to 1–3 g for a 70 kg person. This is within clinical dosing parameters for antibiotics, which are routinely given at such doses two to three times daily for systemic infections; intravenous immunoglobulins may be given in doses up to 150–300 g for a 70 kg person. As pharmacokinetic clearance is substantially slower in humans compared to mice, similar contrast may be achieved using a lower dose of NP41 or related contrast agent although slower pharmacokinetics may increase lead time required before surgery. In addition to improving affinity/specificity of NP41 the attachments of macro-molecular carriers or other controlled released formulation may be required to optimize this contrast agent for potential clinical use.

## Methods

Methods and any associated references are available in the online version of the paper at <http://www.nature.com/naturebiotechnology/>.

## Supplementary Material

Refer to Web version on PubMed Central for supplementary material.

## Acknowledgments

We are indebted to members of our laboratory for discussions and comments on the manuscript. Results described here are being used in support of a patent filing by the University of California, San Diego. This work was supported by the Howard Hughes Medical Institute, grants from the Burrough-Wellcome Fund (Career Award for Medical Scientists) and National Institutes of Health (NIH, 5K08EB008122) to Q.T.N. and NIH grant NS27177 to R.Y.T.

## References

1. Gantz BJ. Intraoperative facial nerve monitoring. *Am. J. Otol.* 1985 Nov.(Suppl.):58–61. [PubMed: 4073246]
2. Davis WE, Rea JL, Templer J. Recurrent laryngeal nerve localization using a microlaryngeal electrode. *Otolaryngol. Head Neck Surg.* 1979; 87:330–333. [PubMed: 492705]
3. Miller MC, Spiegel JR. Identification and monitoring of the recurrent laryngeal nerve during thyroidectomy. *Surg. Oncol. Clin. N. Am.* 2008; 17:121–144. [PubMed: 18177803]
4. Walz J, Graefen M, Huland H. Basic principles of anatomy for optimal surgical treatment of prostate cancer. *World J. Urol.* 2007; 25:31–38. [PubMed: 17333199]
5. Walz J, et al. A critical analysis of the current knowledge of surgical anatomy related to optimization of cancer control and preservation of continence and erection in candidates for radical prostatectomy. *Eur. Urol.* 2010; 57:179–192. [PubMed: 19931974]
6. Kübler HR, et al. Impact of nerve sparing technique on patient self-assessed outcomes after radical perineal prostatectomy. *J. Urol.* 2007; 178:488–492. [PubMed: 17561133]
7. Zhivov A, Blum M, Guthoff R, Stachs O. Real-time mapping of the subepithelial nerve plexus by in vivo confocal laser scanning microscopy. *Br. J. Ophthalmol.* 2010; 94:1133–1135. [PubMed: 20813752]
8. Zysk AM, Nguyen FT, Oldenburg AL, Marks DL, Boppart SA. Optical coherence tomography: a review of clinical development from bench to bedside. *J. Biomed. Opt.* 2007; 12:051403. [PubMed: 17994864]
9. Kobbert C, et al. Currents concepts in neuroanatomical tracing. *Prog. Neurobiol.* 2000; 62:327–351. [PubMed: 10856608]
10. Richmond FJR, et al. Efficacy of seven retrograde tracers, compared in multiple labelling studies of feline motoneurons. *J. Neurosci. Methods.* 1994; 53:35–46. [PubMed: 7527476]
11. Marangos N, Illing R, Kruger J, Laszig R. In vivo visualization of the cochlear nerve and nuclei with fluorescent axonal tracers. *Hear. Res.* 2001; 162:48–52. [PubMed: 11707351]
12. O'Malley M, et al. Fluorescent retrograde axonal tracing of the facial nerve. *Laryngoscope.* 2006; 116:1792–1797. [PubMed: 17003730]
13. Pasqualini R, Ruoslahti E. Organ targeting in vivo using phage display peptide libraries. *Nature.* 1996; 380:364–366. [PubMed: 8598934]
14. Shtatland T, Buettler D, Kossodo M, Pivovarov M, Weissleder R. PepBank—a database of peptides based on sequence text mining and public peptide data sources. *BMC Bioinformatics.* 2007; 8:280. [PubMed: 17678535]
15. Berger S, Bannantine JP, Griffin JFT. Autoreactive antibodies are present in sheep with Johne's disease and cross-react with *Mycobacterium avium* subsp. *Paratuberculosis* antigens. *Microbes Infect.* 2007; 9:963–970. [PubMed: 17544799]



16. Kim GS, et al. Suppression of receptor-mediated apoptosis by death effector domain recruiting domain binding peptide aptamer. *Biochem. Biophys. Res. Commun.* 2006; 343:1165–1170. [PubMed: 16581027]
17. Jiang Y, et al. Targeting of hepatoma cell and suppression of tumor growth by a novel 12mer peptide fused to superantigen TSST-I. *Mol. Med.* 2006; 12:81–87. [PubMed: 16953561]
18. Feng G, et al. Imaging neuronal subsets in transgenic mice expressing multiple spectral variants of GFP. *Neuron.* 2000; 28:41–51. [PubMed: 11086982]
19. Olson ES, et al. Activatable cell penetrating peptides attached to nanoparticles: dual probes for fluorescence and magnetic resonance imaging of proteases in vivo. *Proc. Natl. Acad. Sci. USA.* 2010; 107:4311–4316. [PubMed: 20160077]
20. Nguyen QT, et al. Surgery with molecular fluorescence imaging using activatable cell penetrating peptides decreases residual cancer and improves survival. *Proc. Natl. Acad. Sci. USA.* 2010; 107:4317–4322. [PubMed: 20160097]
21. Osuchowski MF, Teener J, Remick D. Noninvasive model of sciatic nerve conduction in healthy and septic mice: reliability and normative data. *Muscle Nerve.* 2009; 40:610–616. [PubMed: 19618431]

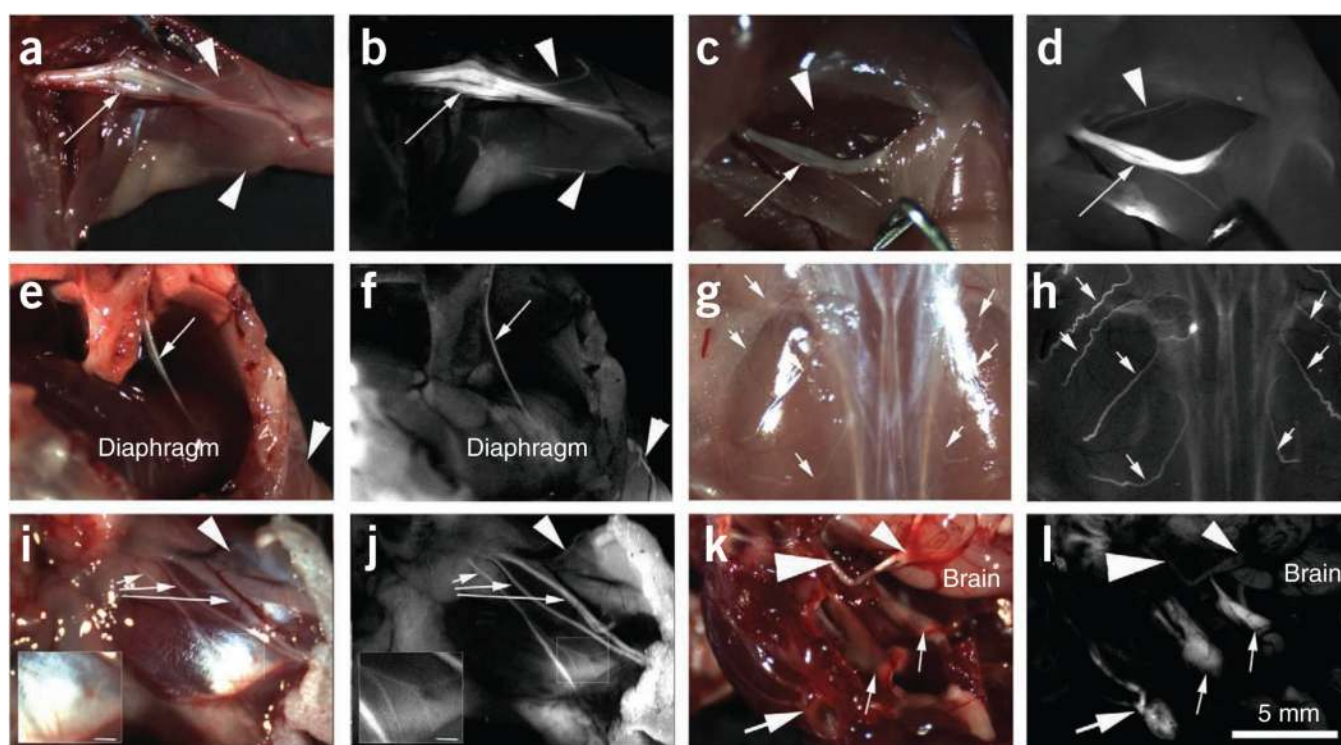


**Figure 1.**

Whole-body survey of nerves in mice ( $n = 3$ ) 4 h after injection with 450 nmoles of FAM-NP41. **(a,b)** Brachial plexus. Reflectance image **(a)** showing left brachial plexus (arrow). Smaller branches ( $\sim 50$ – $100 \mu\text{m}$ ) are easily seen (arrowheads) with fluorescence labeling **(b)** but not in reflectance image. **(c,d)** Sciatic nerve. Reflectance image **(c)** showing right sciatic nerve (arrow). Many more small branches ( $\sim 50$ – $100 \mu\text{m}$ ) are seen (arrowheads) with fluorescence imaging **(b)** compared to reflectance. **(e,f)** Phrenic nerve. Reflectance image **(e)** showing left phrenic nerve (arrow) descending from the mediastinum to innervate the diaphragm. Note that the nerve is seen as a single linear fluorescent structure (arrow, **f**) compared to the bundle of nerve and connective tissue seen with reflectance (arrow, **e**). Arrowhead points to an intercostal nerve which is easily seen with fluorescence but not with reflectance. **(g,h)** Dorsal cutaneous nerves. Reflectance image **(g)** showing the dorsal musculature. Fluorescence imaging highlights the dorsal intercostal nerves (arrows, **h**) that are not easily seen with reflectance. **(i,j)** Facial nerve. Main facial nerve branches (arrows) are easily seen with both reflectance **(i)** and fluorescence **(j)**. However, a small branch of nerve arborization (arrowhead) leading to the upper face can be distinguished from surrounding tissue with fluorescence but not with reflectance. Insert shows arborizations ( $\sim 50 \mu\text{m}$  diameter) of the lower division of the facial nerve that can be easily seen with fluorescence labeling. **(k,l)** Dorsal view of skull base. Reflectance image **(k)** showing left facial nerve (large arrow) wrapping around the ear, trigeminal nerves (small arrows), optic nerves (large arrowhead) and optic chiasm (small arrowhead). Fluorescence image **(l)** shows fluorescence labeling of the facial and trigeminal nerves (peripheral nervous system) but not the optic nerves and chiasm (central nervous system). Scale bar **(a–l)**, 5 mm; inserts **(i and j)**, 1 mm.



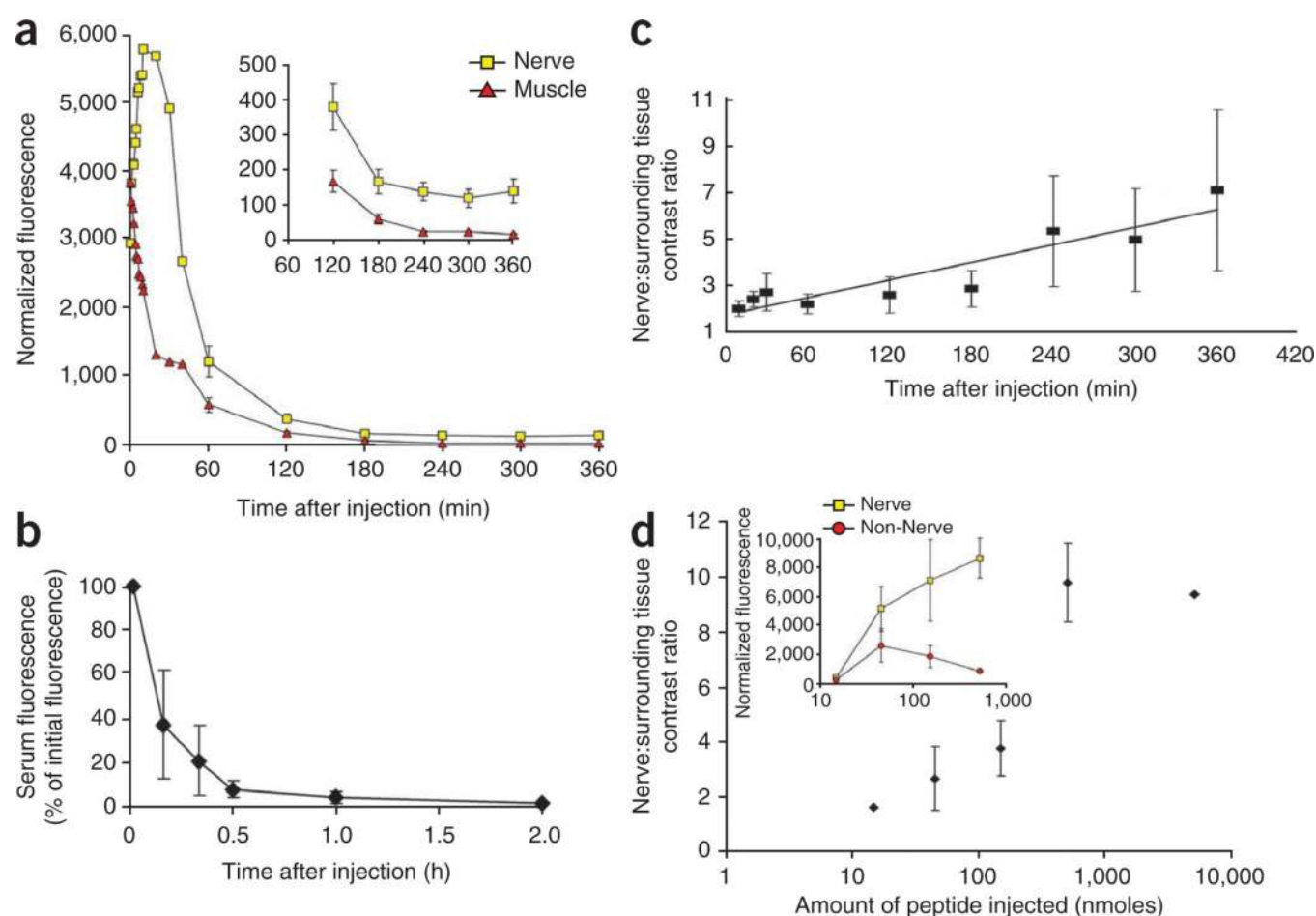


**Figure 2.**

Time course and dose response of FAM-NP41 binding to nerve and nonnerve tissue. **(a–d)** Nerve fluorescence peaked at around 10 min after administration **(a)**, then declined (half-life ~50 min) to a plateau sustained between 3 and 6 h (see inset with expanded intensity scale, Student's *t*-test, two-tailed,  $P = 0.002$  at 2 h, 0.0007 at 3 h, 0.0007 at 4 h, 0.003 at 5 h, 0.006 at 6 h). In contrast, muscle fluorescence was highest immediately after intravenous administration of the peptide, then declined steadily with a half-life of ~20 min **(a)**. Serum half-life was calculated at ~10 min **(b)**. Useful contrast between nerve and surrounding muscle developed by 2 h and lasts several hours **(c)**. Nerve-to-surrounding tissue contrast ratio increased with increasing amount of peptide injected, concentration from 15 to 5,000 nmoles per mouse injected ( $n = 2$ ) **(d)**, because surrounding nonnerve tissue fluorescence seems more saturable than nerve binding with increasing peptide concentration (inset).

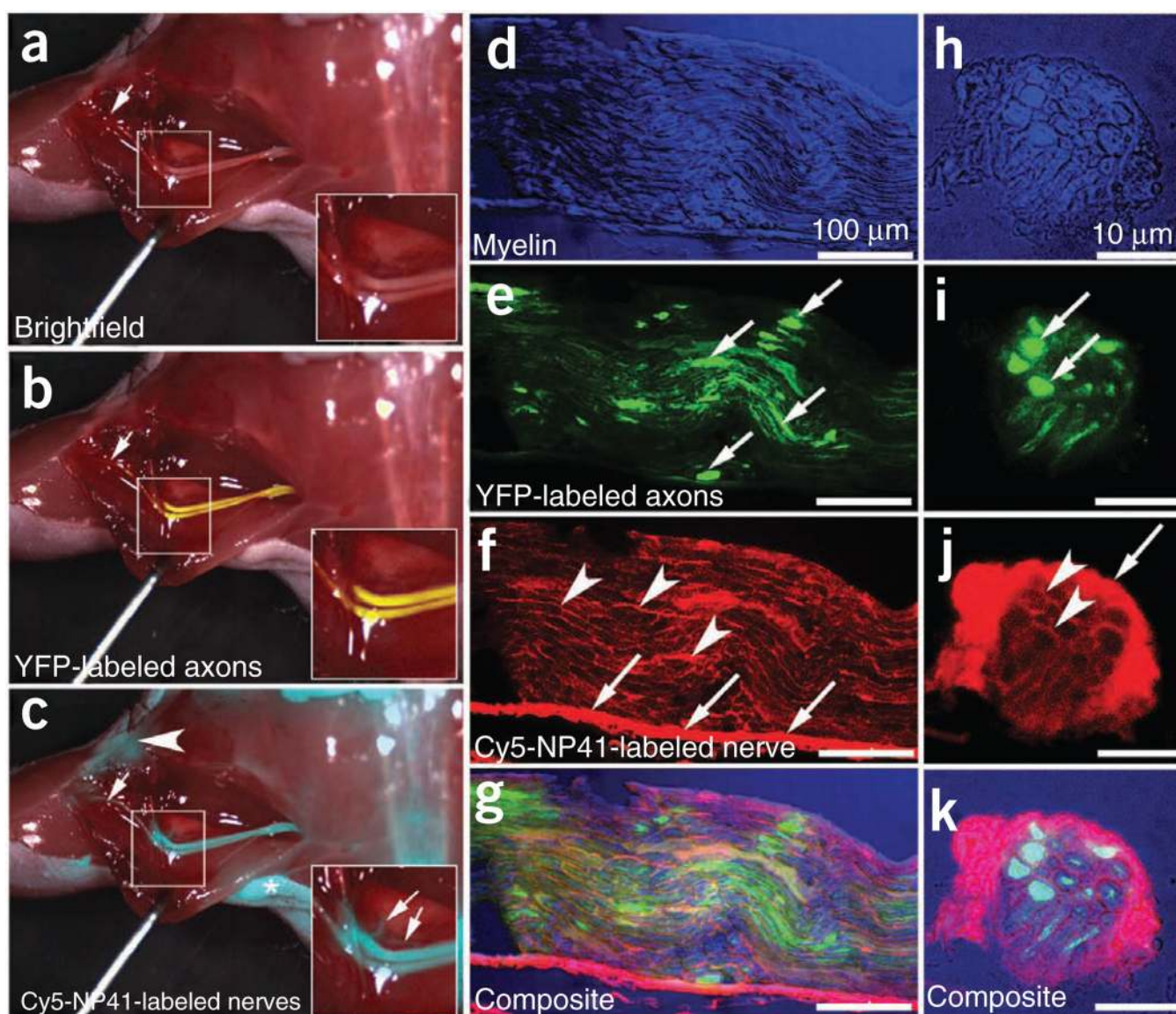


**Figure 3.**

Cy5-NP41 (acetyl-SHSNTQTLAKAPEHTGC-(Cy5)-amide) labeling of sciatic nerve in Thy1-YFP transgenic mice. **(a)** Low-power brightfield view of left exposed sciatic nerve. Inset shows magnified view of central boxed region. **(b)** Same nerve as in **a** with YFP fluorescence (pseudocolored yellow) superimposed on the brightfield image, showing transgenic expression of YFP in axons. **(c)** Same nerve as in **a** and **b** viewed with Cy5 fluorescence (pseudocolored cyan for maximal contrast during live surgery) superimposed on the brightfield image, showing nerve labeling with Cy5-NP41. Arrows in **b** and **c** point to thin buried nerve branches that are better revealed by the long-wavelength Cy5 fluorescence than by brightfield reflectance or shorter-wavelength YFP fluorescence. There is some nonspecific labeling of skin (asterisk) and cut edges of muscle (arrowhead) by Cy5-NP41. Fortunately, such nonspecific labeling hardly ever has the filamentous appearance of nerves, so an experienced surgeon can usually distinguish nonspecific from specific targets. **(d)** Low magnification longitudinal section showing myelin within the sciatic nerve using differential interference contrast (DIC), pseudocolored blue. **(e)** Same nerve as in **d** showing axoplasmic

YFP pseudocolored green (arrows). **(f)** Same nerve as in **d** and **e**, showing Cy5-NP41 labeling (pseudocolored red) of epineurium (arrows) and endoneurium (arrowheads). **(g)** Composite image of **d**, **e** and **f** showing that NP41 labeling does not colocalize with either myelin or axoplasm. **(h–k)** Cross-sectional images corresponding to panels **e–g**.

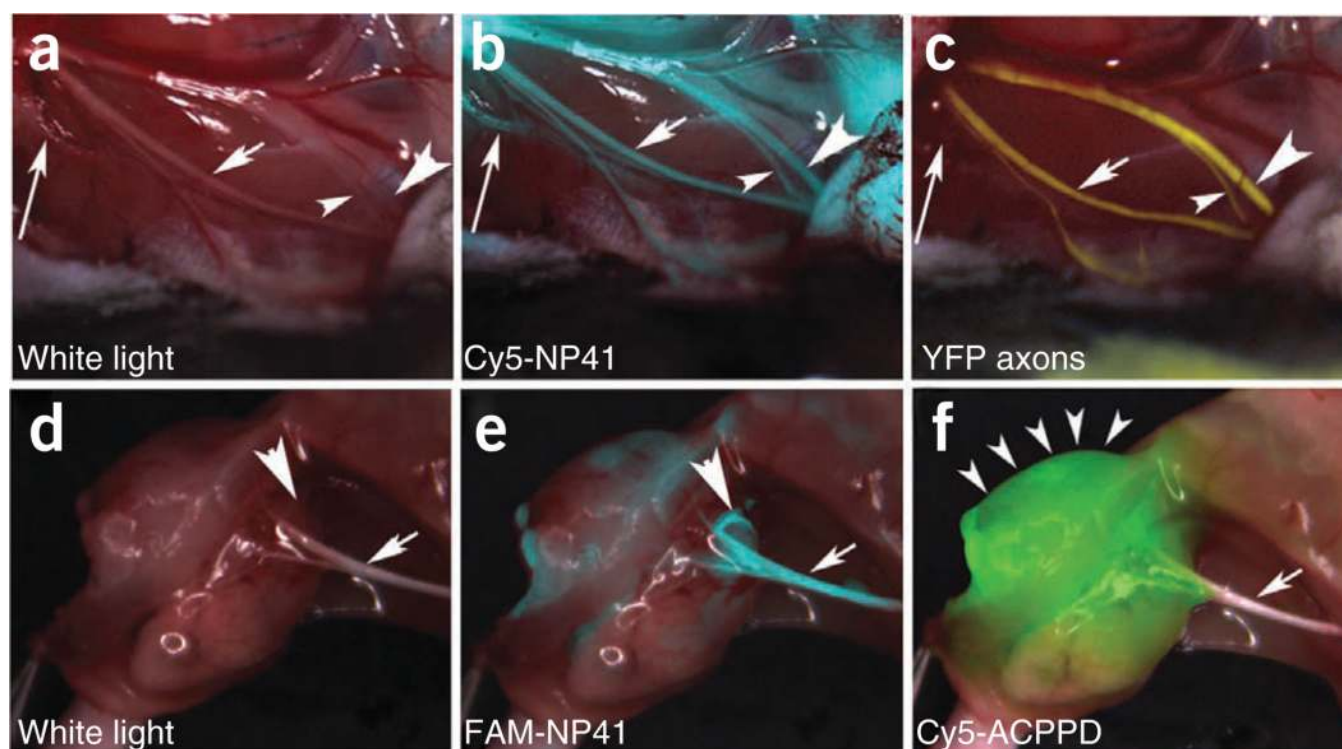


**Figure 4.**

NP41 can highlight buried nerve branches invisible by standard illumination. **(a–c)** Right facial nerve and its arborizations in a thy1-YFP mouse treated with Cy5-NP41, viewed by **(a)** white light reflectance, **(b)** Cy5 fluorescence (pseudocolored cyan) overlaid on reflectance and **(c)** YFP fluorescence (pseudocolored yellow), also overlaid on reflectance. The short arrow marks a nerve branch visible by all three imaging modes. The arrowheads point to branches that are difficult to differentiate from muscle fascia in reflectance, but clearly distinguishable in both fluorescence images. The long arrow indicates a deeply buried branch visible only by Cy5-NP41 due to the better penetration of far-red wavelengths. **(d–f)** Left sciatic nerve (arrow) and its arborization in a mouse with a syngeneic 8119 mammary tumor graft<sup>17,18</sup>, viewed by **(d)** white light reflectance, **(e)** FAM fluorescence 2 h after intravenous injection of NP41 (150 nmoles) (pseudocolored cyan, overlaid on reflectance) and **(f)** Cy5 fluorescence (pseudocolored green, overlaid on reflectance) from conjugates of activatable cell-penetrating peptides and dendrimers (ACPPDs). The large arrowheads in **d** and **e** point to a nerve branch buried under tumor, visible only by FAM fluorescence. Small arrowheads in **f** denote tumor. See Supplementary Video 1.